Molecular Simulation on the Thermal Stability of Meta-Aramid Insulation Paper Fiber at Transformer Operating Temperature

Chao Tang [1,*] **, Xu Li** [1,2] **, Zhiwei Li** [1,3] **, Wenxin Tian** [1] **and Qu Zhou** [1]

[1] College of Engineering and Technology, Southwest University, Chongqing 400715, China; swugzlx@163.com (X.L.); ccqepc@163.com (Z.L.); 13657601997@163.com (W.T.); zhouqu@swu.edu.cn (Q.Z.)
[2] Zunyi Power Supply Bureau, Zunyi 563000, China
[3] Wuxi County Power Supply Branch of State Grid Chongqing Electric Power Company, Chongqing 405800, China
[*] Correspondence: tangchao_1981@163.com; Tel.: +86-23-6825-1265

Abstract: The influence of the thermal field of a transformer during operation on the thermal stability of meta-aramid insulation paper was studied through molecular dynamics simulations. Models of the crystalline and amorphous regions of meta-aramid fibers were constructed using known parameters. The model of the crystalline area was verified by comparing X-ray diffraction results with experimental data. The reasonableness of the simulation results was judged by the variation of energy, temperature, density, and cell size in relation to the dynamic time. The molecular dynamics simulations revealed that the modulus values in the crystalline regions were two to three times higher than those in the amorphous regions at various temperatures. In addition, the incompressibility, rigidity, deformation resistance, plasticity, and toughness of the crystalline regions were obviously higher than those of amorphous regions, whereas the toughness of the amorphous regions was better than that of the crystalline regions. The mechanical parameters of both the crystalline and amorphous regions of meta-aramid fibers were affected by temperature, although the amorphous regions were more sensitive to temperature than the crystalline regions. The molecular chain motion in the crystalline regions of meta-aramid fibers increased slightly with temperature, whereas that of the amorphous regions was more sensitive to temperature. Analyzing hydrogen bonding revealed that long-term operation at high temperature may destroy the structure of the crystalline regions of meta-aramid fibers, degrading the performance of meta-aramid insulation paper. Therefore, increasing the crystallinity and lowering the transformer operating temperature may improve the thermal stability of meta-aramid insulation paper. However, it should be noted that increasing the crystallinity of insulation paper may lower its toughness. These study results lay a good foundation for further exploration of the ways to improve the performance of meta-aramid insulation paper.

Keywords: meta-aramid insulation; thermal stability; mechanical parameter; chain motion; hydrogen bonding

1. Introduction

Aramid paper was developed by Du Pont in the 1960s and called Nomex paper. Aramid paper was produced from Nomex short-cut fibers and aramid pulp as raw materials using an oblique net papermaking wet method [1]. Although aramid fibers are synthesized artificially, their structure and that of naturally occurring cellulose both include regions with crystalline structure and amorphous structure.

The crystalline content of meta-aramid fibers is low; they possess an amorphous content of 75–80% [2]. The crystallinity of aramid short-cut fibers and pulp were measured by Liao Ruijing [3]. The results showed that the crystallinity of aramid short-cut fibers was 13.17%, whereas the crystallinity of aramid pulp was only 1.53%. In contrast, the crystallinity of self-made aramid insulation paper is much higher [1]; after hot pressing, the crystallinity of self-made aramid paper is 35.04%, while that of Nomex paper is 43.43%, and the crystallinity of self-made pure aramid pulp paper after hot pressing is 7.2%. The crystallinity of meta-aramid fibers prepared by Zhiqing [4] ranged from 29% to 41%. Therefore, the amorphous regions represent the major component of the molecular structure of both Nomex paper, which has the best performance in the industry, and aramid insulation paper prepared in a laboratory. Both the crystalline and amorphous regions in insulation paper are important to its performance. However, the performance of the crystalline and amorphous regions of meta-aramid fibers has not been comprehensively studied, particularly their microscopic behavior at the molecular and atomic levels.

Aging and the performance improvement of polymers have become hot research topics [5–7]. Thermal aging is one of the major types of aging of insulation paper inside a transformer. In recent years, numerous studies have focused on the thermal aging mechanism of insulation paper. Although the aging process and its mechanism on oil–paper in transformers have been investigated [8–18], the thermal stability of meta-aramid insulation paper in transformers at operating temperature has not been analyzed. Therefore, it remains important to examine the thermal stability and thermal aging mechanism of crystalline and amorphous regions in meta-aramid insulation paper.

In this paper, a molecular dynamics simulation method [19–27] is used to conduct a comparative analysis of the influence of a thermal field on the thermal stability of crystalline and amorphous regions of meta-aramid fiber from the perspective of an actual thermal field environment inside a transformer. First, we construct a model of meta-aramid with crystalline and amorphous regions using reported experimental data. Then, we use a molecular dynamics method to conduct geometry optimization, annealing of the model, and dynamics simulations. Finally, we analyze the influence of different temperatures on the mechanical parameters, chain motion, and hydrogen bonding of the model. This paper lays a foundation for further study on how to improve the performance of meta-aramid insulation paper.

2. Materials and Methods

2.1. Model Construction

2.1.1. Construction of a Model of the Crystalline Area of Meta-Aramid Insulation Paper

In molecular dynamics, the first and one of the most major steps is model construction; the reliability and effectiveness of simulation results depend on model construction and processing. It is known from X-ray diffraction (XRD) analysis that the crystal structure of meta-aramid fibers is triclinic with specific unit cell parameters of a = 0.527 nm, b = 0.525 nm, c = 1.13 nm (fiber axis), α = 111.5°, β = 111.4°, and γ = 88.0° [28,29]. In addition, the microstructure of meta-aramid fibers is fibrillar. The chain number of meta-aramid fibers in the unit cell is taken to be one, and it was calculated from the crystal structure that the density of the crystalline area is ρ = 1.47 g/cm^3. When meta-aramid fibers are crystallized, each molecular unit shrinks by 0.1 nm, and the angle between the planes of the benzene ring and adjacent amino group is about 30°. In addition, the space group of meta-aramid fibers is P1 [29]. The model that we constructed based on this reported information is shown in Figure 1a–c. Fractional atomic coordinates were used in the model of the crystalline area of meta-aramid fibers constructed in this paper. All models are created using the Materials Studio 5.0 Building Tool software.
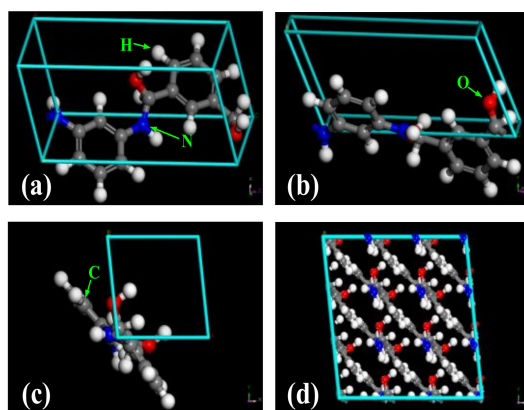
Figure 1. Meta-aramid fiber crystal model. (**a**) and (**b**) Side views of the unit cell in the meta-aramid fiber crystalline area, (**c**) front view of the unit cell in the meta-aramid fiber crystalline area, and (**d**) front view of the supercell.

Tanala et al. [30] calculated a crystal model of cellulose Iβ based on reported data [31]. They found that the dimensions of the force field and model influenced the calculated result for a tensile modulus by calculating the mechanical performance of models with different sizes: $1 \times 1 \times 10$ and $4 \times 4 \times 10$ unit cells. It was pointed out in their paper that a supercell is more rational than a primitive cell. Therefore, this paper uses a supercell model to calculate the crystal parameters of meta-aramid fibers. The $3 \times 3 \times 2$ supercell model constructed using a supercell module is shown in Figure 1d. The supercell has unit cell parameters of $a = 1.581$ nm, $b = 1.575$ nm, $c = 2.26$ nm, $\alpha = 111.5°$, $\beta = 111.4°$, and $\gamma = 88.0°$. In the constructed crystal models, the chain numbers in the unit cell and supercell are one and nine, respectively.

2.1.2. Assessment of the Constructed Model

To verify the model, the powder diffraction module in a Reflex diffractometer was used to conduct XRD experiments. XRD parameters were set as follows: the 2θ range was 5°–45°, the step size was 0.05°, and copper was used as the X-ray source. The XRD pattern for the supercell, which is shown in Figure 2a, contained peaks at 9.1°, 17°, 18.3°, 20.4°, 23.4°, and 27.4°. The reported [32] XRD pattern for meta-aramid fibers contained diffraction peaks at 11°, 18°, 24°, and 28°. The difference of crystallinity of different fiber samples was detected by comparing the intensities of corresponding diffraction peaks, which revealed that the results in this paper are similar to Wen Yang [32]. Therefore, the model of the crystalline area of meta-aramid fibers that is constructed in this paper is reasonable.

The stability of a model structure needs to be assessed after construction. In this paper, the stability of the model was determined by examining the changes of energy, temperature, density, cell length, and other parameters of the model during the molecular dynamics simulation time. In the molecular dynamics simulations, energy and temperature fluctuated by 5–10%, showing that the model structure was successfully optimized, and the system reached a balanced state [33,34], allowing subsequent dynamics simulations to be conducted. The changes of crystalline area parameters of the model after geometry optimization and annealing during the simulation time at room temperature (298 K, 25 °C) are shown in Figure 2b–d.

Figure 2b–d respectively reveal that the energy, temperature, and density of the model all slightly fluctuated during the simulation time. The cell length of the model also fluctuated. Figure 2c illustrates that the steady-state values of temperature and density are 298 K and 1.44 g/cm³, respectively. The simulated density is slightly lower than the calculated value by Wen Yang [32], which resulted from the flaccid supercell structure during the relaxation process. The steady-state cell lengths along the X, Y, and Z axes are 1.598 nm, 1.594 nm, and 2.285 nm, respectively. These values are slightly larger than those of the initial model, which again results from the flaccid model structure during the relaxation process. Generally, the changes of the unit cell parameters of the model during the

simulation time are small. After geometry optimization and annealing, the energy, temperature, density, and cell length of the model of the crystalline area of meta-aramid fibers fluctuated slightly during the simulation time. Therefore, it is believed that the model reached a balanced state, allowing further simulations to be conducted.
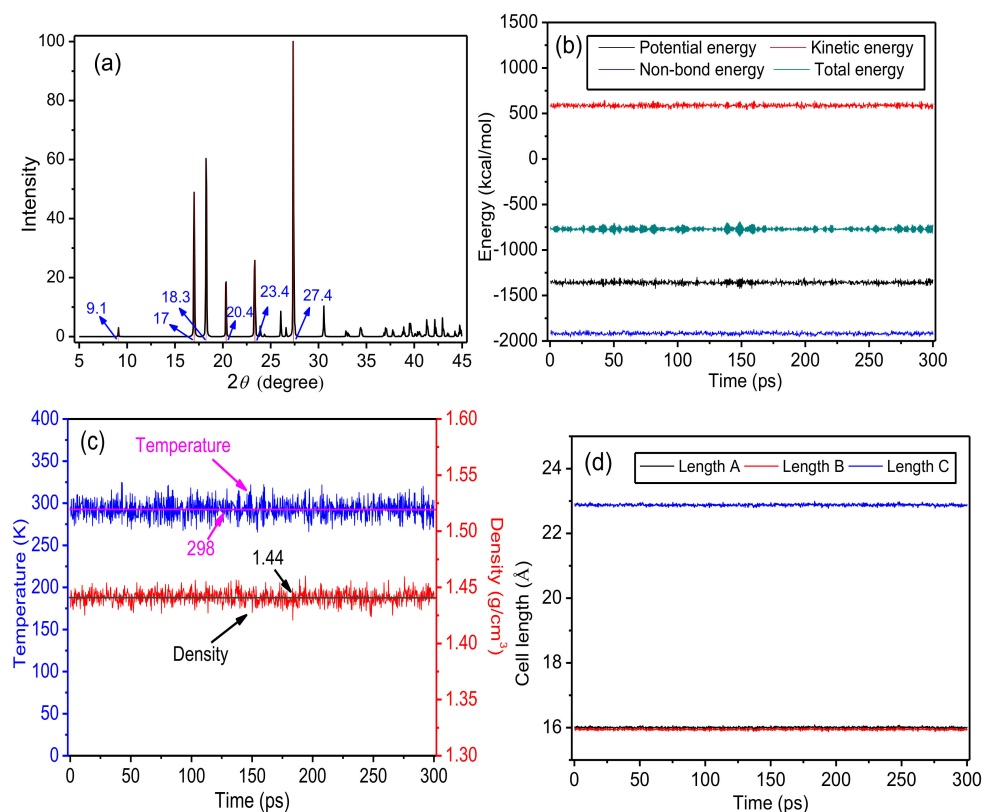

Figure 2. Parameters of the meta-aramid fiber crystal model. (**a**) X-ray diffraction (XRD) pattern of the supercell, (**b**) change of energy during the simulation (1 kcal/mol = 6.9477×10^{-21} J), (**c**) changes of temperature and density during the simulation, and (**d**) change of the unit cell length during the simulation (1 Å = 10^{-1} nm).

2.1.3. Construction of a Model of the Amorphous Area of Meta-Aramid Insulation Paper

The degree of polymerization (DP) of long polymer chains is high; for example, the average DP of cellulose in the insulation paper of new transformers is about 1000 [35]. The molecular weight of meta-aramid fibers is 60,000–90,000 [36], and the molecular chains have a high DP. However, in computer simulations, it is unnecessary to use very long chains during the computing process, which saves computing time and aids the analysis of the main mechanisms governing a system. For example, Mazeau et al. [37] used cellulose chains with different DPs to construct an amorphous model. Their simulation results showed that the models constructed with different chain lengths displayed similar molecular conformations and physicochemical properties. The visualizer module has been used to construct a meta-aramid fiber model with a DP of 10 for the selection and survey of PCFF (polymer consistent force field) and COMPASS (Condensed-phase Optimized Molecular Potentials for Atomistic Simulation Studies) force fields [33]. Another study constructed a meta-aramid fiber model with a DP of four to investigate the interfacial interactions between aramid and silicon dioxide [38]. Previous results show that it is unnecessary to construct a molecular model with the same DP as that of reality, as long as it is guaranteed that the constructed model and selection of simulation parameters are reasonable. For the model of the amorphous area of meta-aramid fibers constructed in this work, the DP was eight, the chain number was eight, and the initial density was 1.0 g/cm^3. An amorphous cell module was used to construct the model. The constructed model is

depicted in Figure 3. The changes of the energy, temperature, density, cell length, and other parameters during the dynamics simulation time were similar to those of the model of the crystalline area, so they are not given here.
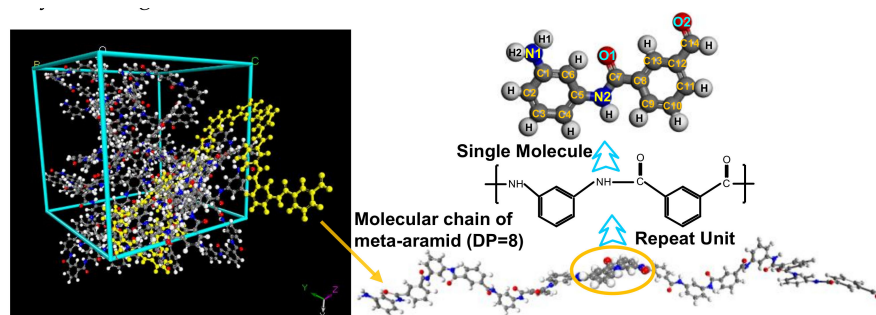

Figure 3. Model of the amorphous area of meta-aramid fibers.

2.2. Simulation Details

Materials Studio (Accelrys, San Diego, CA, USA) software was used to conduct the simulations. The Build Crystals module was employed for model construction, and the Forcite module was used for geometry optimization, annealing, and dynamics simulations with periodic boundary conditions. After each model was constructed, its energy was high, and its structure was in an unstable state. Thus, it was necessary to conduct geometry optimization and then annealing for the various models. The purpose of annealing was to make the model structures more realistic. Fine was selected as the quality of geometry optimization, and the Smart algorithm was used during the optimization process with a maximum iterative step number of 5000, annealing period of 10, and initial temperature of 300 K. The mid-cycle temperature of each period is set as 900 K, and the number of heating ramps per cycle was 10. After optimization and annealing, the rationality of the model structure needed to be assessed. Molecular dynamics simulations were conducted if the model was rational; otherwise, the model was optimized and annealed again until it became rational. Dynamics simulations were conducted for 300 ps in the NVT (Number of particles, Volume and Temperature) ensemble with a step length of 1 fs, truncation radius of 9.5 Å, and spline width of 1 Å. The NVT ensemble was then changed to the NPT (constant pressure and temperature) ensemble using the temperature control method of Nose and pressure control method of Berendsen. The pressure was set as standard atmospheric pressure, the simulation time was 300 ps, and dynamics information was collected every 500 steps. The ambient temperature inside a transformer is generally 363 K, and may increase to about 423 K for short periods. Therefore, the investigated temperature range was 343–423 K. During the simulation process, the target temperatures were 343–423 K with an increment of 20 K. Therefore, five systems were simulated for each model.

3. Mechanical Parameters

3.1. Mechanical Parameters of the Crystalline Regions of Meta-Aramid Insulation Paper

The mechanical parameters of polymers are very important parameters [39]. The change of the mechanical parameters of insulation paper over time is a result of the long-term action of both thermal and electric fields inside the transformer. Therefore, this change can reflect the change of thermal stability of the insulation paper to a certain degree. The general relationship between stress and strain for solid materials can be expressed by the generalized Hooke law considering elasticity [40]. Various mechanical parameters of materials can be calculated based on elasticity, including bulk modulus (K), shear modulus (G), tensile modulus (E), K/G value, Poisson ratio (ν), and Cauchy pressure (C_{12}–C_{44}). These parameters can be used to show the different mechanical properties of a material. The relevance and calculation method of these parameters have been reported

elsewhere [17]. The mechanical parameters of crystalline regions of meta-aramid fibers at different temperatures are summarized in Table 1. Data from the last 20 frames in the trail file were used for statistical analyses.

Table 1. Mechanical parameters (GPa) of the crystalline regions of meta-aramid fibers at different temperatures.

	343 K	363 K	383 K	403 K	423 K
C_{11}	16.0766	15.6049	15.8853	15.4653	15.9172
C_{22}	23.9779	22.4932	23.3769	21.8053	23.8483
C_{33}	125.3986	123.4178	124.6375	122.6217	125.2992
C_{44}	4.5859	4.3149	4.3826	4.2938	4.4550
C_{55}	10.8213	10.2667	10.7308	9.9972	10.7810
C_{66}	4.9536	4.5564	4.8864	4.5042	4.9309
C_{12}	13.0176	12.3408	12.7655	12.0673	12.9137
C_{13}	11.8826	10.9720	11.5453	10.2754	11.7574
C_{23}	11.0271	9.8351	10.5568	9.2691	10.9485
C_{15}	0.7719	0.7950	0.7519	0.9097	0.7905
C_{25}	2.2807	2.1310	2.2902	2.1407	2.2932
C_{35}	-12.6427	-11.4554	-12.1603	-10.8019	-12.6015
C_{46}	-1.2672	-1.2086	-1.2434	-1.1815	-1.2688
K	15.0370	14.4768	14.8211	14.2173	14.8985
G	4.5149	4.3324	4.4061	4.2939	4.4462
E	12.3125	11.8183	12.0265	11.7034	12.1319
ν	0.3635	0.3639	0.3648	0.3628	0.3643
$C_{12}-C_{44}$	0.2380	0.2498	0.2445	0.2516	0.2424
K/G	3.3305	3.3415	4.4061	3.3111	3.3508

Except for C_{35}, the values of C_{15}, C_{25}, and C_{46} calculated for various temperature conditions were close to 0, showing that the meta-aramid fiber crystals are not strongly anisotropic elastomers. Three groups were observed: C_{11}, C_{22}, and C_{33} in Group 1; C_{44}, C_{55}, and C_{66} in Group 2; and C_{12}, C_{13}, and C_{23} in Group 3. The difference between the values in groups 2 and 3 was small, whereas the variation between the values in Group 1 was large, showing that the crystalline regions of meta-aramid fibers behave as anisotropic elastomers. The Cauchy pressure is positive, showing that the toughness of crystalline regions of meta-aramid fibers is high.

The mechanical parameters of crystalline regions of meta-aramid fibers are similar at different temperatures, showing that the influence of temperature on the mechanical performance of crystalline regions of meta-aramid fibers is small within the operating temperature range of a transformer. However, the bulk modulus, shear modulus, and tensile modulus at 343 K are higher than those at other temperatures, showing that the incompressibility, rigidity, and capacity to resist deformation of the crystalline regions of meta-aramid fibers are weakened at this temperature. Of all the investigated mechanical parameters of the crystalline regions of meta-aramid fibers, the change of ν is the smallest; that is, the plasticity of these regions is only slightly influenced by temperature.

3.2. Mechanical Parameters of the Amorphous Regions of Meta-Aramid Fibers

The mechanical parameters of amorphous regions of meta-aramid fibers at different temperatures are given in Table 2. The C_{15}, C_{25}, C_{35}, and C_{46} values obtained at various temperatures are close to 0, showing that the amorphous regions of meta-aramid fibers are not strongly anisotropic elastomers. The values for the groups of C_{11}, C_{22}, and C_{33}; C_{44}, C_{55}, and C_{66}; and C_{12}, C_{13}, and C_{23} are very close, indicating that the amorphous regions of meta-aramid fibers are isotropic elastomers. This is different from the crystalline regions of the meta-aramid fibers, which are anisotropic elastomers; this difference is caused by their different molecular arrangements.

Various modulus values in Table 2 decreased with increasing temperature, showing that the rise of temperature weakens the incompressibility, rigidity, and the capacity to resist the deformation of the amorphous regions. The change of Poisson ratio is generally small, showing that the plasticity of the amorphous regions is only slightly influenced by temperature. The values of Cauchy pressure

at different temperatures are positive and increase with temperature, revealing that the elevated temperature increases the fragility of amorphous regions of meta-aramid fibers and strengthens their toughness. The change of K/G value with temperature is not obvious, showing that the toughness of the amorphous regions is not greatly influenced by temperature.

The modulus values of crystalline regions are two to three times higher than those of the amorphous regions at the various temperatures. This shows that an increased degree of crystallinity can improve the mechanical performance of meta-aramid insulation paper in many ways. In particular, the incompressibility, rigidity, and the capacity of the crystalline regions to resist deformation are obviously higher than those of the amorphous regions. The Poisson ratios and K/G values of the crystalline regions are obviously higher than those of the amorphous regions, revealing that the plasticity and toughness of the crystalline regions are obviously better than those of the amorphous regions. Meanwhile, the Cauchy pressure values of the amorphous regions are obviously higher than those of the crystalline regions, showing that the toughness of the crystalline regions is better than that of the amorphous regions. Thus, the crystalline and amorphous regions of meta-aramid fibers have different performances under a thermal field. Within the temperature range that was used in this paper, the crystalline regions maintain pretty good mechanical performance at the different temperatures, and their modulus values are not greatly influenced by temperature. In comparison, the amorphous regions are more sensitive to temperature; the higher the temperature, the lower the modulus value. This is because the crystalline regions have a pretty stable molecular structure, whereas the molecular chains of the amorphous regions have a low degree of regularity or even random arrangement.

Table 2. Mechanical parameters (GPa) of the amorphous regions of meta-aramid fibers at different temperatures.

	343 K	363 K	383 K	403 K	423 K
C_{11}	8.1447	7.9929	5.1929	5.6865	6.8282
C_{22}	8.9980	7.5829	8.4336	7.0976	6.3522
C_{33}	7.2241	5.9593	4.9543	4.5814	2.0924
C_{44}	2.2998	1.7513	1.8466	2.2429	1.5376
C_{55}	2.0434	1.2013	1.6225	0.9254	0.9510
C_{66}	2.8573	2.0955	1.7349	1.6217	1.8102
C_{12}	3.8344	2.9190	3.0527	2.4052	2.5152
C_{13}	2.4708	2.1749	1.7479	1.6032	0.8586
C_{23}	3.6596	2.4105	2.5815	2.3323	1.4437
C_{15}	-0.0694	0.8525	-0.0942	0.3096	0.5644
C_{25}	-0.3623	0.5968	-0.0516	-0.3104	0.0129
C_{35}	0.1970	0.9408	-0.1131	-0.3859	0.4334
C_{46}	-0.0433	0.0407	0.0788	-0.0223	-0.1534
K	4.6983	3.3653	3.2997	3.1083	1.5984
G	2.3164	1.7035	1.7287	1.3537	1.1772
E	5.9683	4.3728	4.4152	3.5463	2.8354
ν	0.2883	0.2834	0.2770	0.3098	0.2043
C_{12}–C_{44}	0.4320	0.6818	0.5838	0.8279	0.8389
K/G	2.0283	1.9755	1.9087	2.2961	1.3578

4. Chain Motion

4.1. Chain Motion of Crystalline Regions of Meta-Aramid Fibers

Chain motion in polymers strongly influences their thermal stability. Mean square displacement (MSD) can be used to characterize the chain motion of a polymer; the larger the slope of an MSD time curve, the more severe the chain motion of a polymer, and the poorer its thermal stability. Curves with

the same trend can be directly judged based on values; namely, the larger the MSD value, the greater the chain motion. The relation between MSD and time [41,42] can be shown as:

$$MSD = \left\langle \left| \vec{r}_i(t) - \vec{r}_i(0) \right|^2 \right\rangle \tag{1}$$

In Equation (1), $\vec{r}_i(t)$ is the position vector of atom *i* at time *t* in the system, and $\vec{r}_i(0)$ is the initial position vector of the atom.

Figure 4 presents MSD time curves for crystalline regions of meta-aramid fibers at different temperatures. The trend of the chain motion of molecules in the crystalline regions over time is the same at different temperatures. With rising temperature, the chain motion of crystalline regions of meta-aramid fibers increased slightly. While the increase of chain motion is small, it shows pretty strong temperature dependence, which is especially obvious at about 250 ps. The main reason for this is that the influence of temperature on the physicochemical properties of crystalline regions of meta-aramid fibers was small in the temperature range studied here, showing that the crystal structure of meta-aramid fibers has good stability when exposed to the operating temperature inside a transformer for a long period.

The changes of total energy and non-bond energy during the simulations at different temperatures are displayed in Figure 5. Figure 5a reveals that with lengthening simulation time, the model energy remained in dynamic balance, showing that the previous optimization achieved its expected purpose. The molecular kinetic energy increases with temperature, and the total energy of the model also increases. Figure 5b illustrates that although the non-bond energy of the model increases with temperature, the difference in the non-bond energy at different temperatures is small. Therefore, the influence of the thermal field in the temperature range that was used in this work on the van der Waals interactions inside the crystalline regions is small.
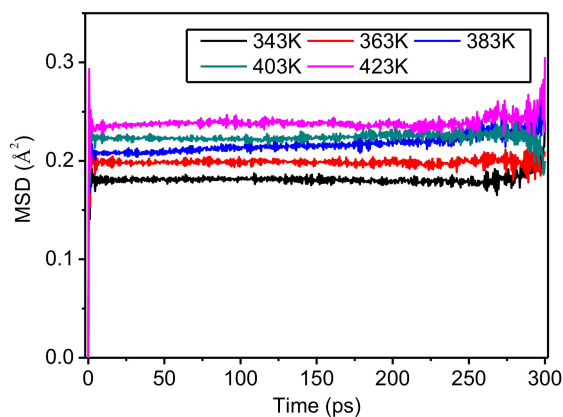

Figure 4. Mean square displacement (MSD) of crystalline regions of meta-aramid fibers at different temperatures.
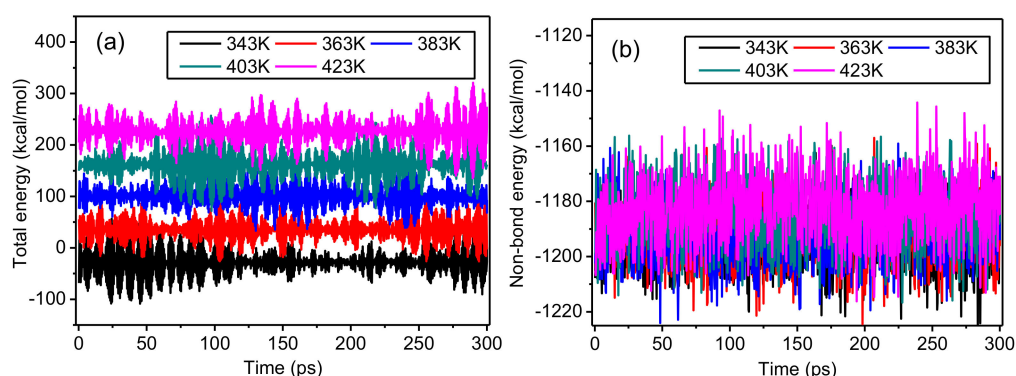
Figure 5. Changes of (**a**) total energy and (**b**) non-bond energy during the simulations at different temperatures.

The relationships between the density of the crystalline regions and simulation time at different temperatures are given in Figure 6. Within the simulation time of 300 ps, the density changed within the range of 1.48–1.505 g/cm^3 without obvious fluctuation, showing again that the model is reliable during this period. The curves overlap because of the small differences in density, indicating that density is not strongly influenced by temperature; in addition, this result also shows that the crystalline regions of meta-aramid fibers have high thermal stability.

Figure 6. Change of the density in the crystalline regions of meta-aramid fibers during the simulations at different temperatures.

Overall, the simulation results showed that the molecular chain motion of crystalline regions of the meta-aramid fibers increased only slightly under the action of a thermal field. The kinetic energy of molecular chains increased with temperature, and the total energy also increased; however, the non-bond energy in the force field expression was not strongly influenced by temperature. The density of crystalline regions remained similar at different temperatures. Therefore, the crystalline regions maintained high thermal stability in the temperature range that was investigated in this paper.

4.2. Chain Motion of Amorphous Regions of Meta-Aramid Fibers

The MSD time curves for the amorphous regions of meta-aramid fibers at different temperatures are shown in Figure 7. The molecular chain motion of amorphous regions showed a positive correlation with temperature. When the temperature was low, the increase of the MSD of the amorphous regions was slow. Conversely, when the temperature was high, the increase of MSD was rapid, which was manifested as a steeper curve, indicating the stronger molecular chain motion of the amorphous regions at higher temperature. Comparing the curves revealed that the MSD time curves at 343 K and 363 K were similar. After about 225 ps, the higher the temperature, the lower the curve, and the larger

the difference between the MSD values of all of the curves. These results show that the molecular chain motion in the amorphous regions is highly sensitive to temperature. Therefore, decreasing the operating temperature of a transformer can effectively improve the thermal stability of amorphous regions of meta-aramid insulation paper.
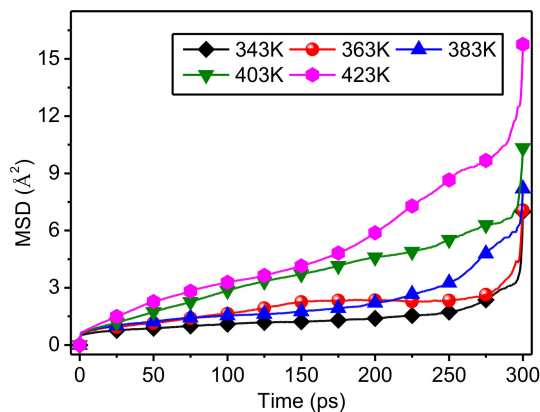

Figure 7. MSD time curves for amorphous regions of meta-aramid fibers at different temperatures.

Comparing the results in Figure 4 and Figure 7 reveals that the chain motions in both the amorphous and crystalline regions of meta-aramid fibers is influenced by temperature; in addition, molecular chain motion and temperature are positively correlated. The MSD values of amorphous regions are obviously higher than those of crystalline regions, showing that the chain motion of amorphous regions in a thermal field is obviously stronger than that of crystalline regions. The sensitivity of the molecular chain motion of amorphous regions to temperature is obviously greater than that of the molecular chains in crystalline regions.

The changes of total energy and non-bond energy for the amorphous regions of the meta-aramid fibers during the simulations at different temperatures are displayed in Figure 8. With the lengthening simulation time, the model energy remains in dynamic balance; namely, it fluctuates around one stable value, showing that the model conformation was sufficiently stable during the early stage of the simulations. The model energies changed with temperature; the total energy and non-bond energy of the model both increased with temperature, indicating that the temperature strongly influences the model energy during the simulation process. Raising the temperature increased both the aramid chain motion and molecular kinetic energy; in addition, the chain space increased, so the molecular potential energy and total energy also increased, conforming to the laws of thermodynamics. Moreover, the non-bond energy also increased with rising temperature, because the van der Waals force between chains increased with the molecular chain motion.

The changes of density of the amorphous regions of meta-aramid fibers during simulations at different temperatures are presented in Figure 9. In the first 105 ps of the simulations, the density of the model increased greatly. After 105 ps, the density did not obviously increase, indicating that the steady-state density is the actual density of the model at a corresponding temperature. The density of the model increased with temperature, which is mainly because the motion of molecular chains strengthened with rising temperature; the model volume also increased. In the NPT ensemble, it is necessary to decrease the model volume V to maintain constant pressure P of particle population N in the model; namely, to fix the model quality. Therefore, the model density was slightly increased. The stronger the motion of molecular chains in the model, the quicker its volume decreases, and the greater the increase of model density. The densities of the model at 343 K, 363 K, and 383 K were similar. In contrast, the densities at 403 K and 423 K were quite different, especially after about 250 ps. This result shows that a higher temperature induces a stronger chain motion in the amorphous regions of the meta-aramid fibers, lowering their thermal stability. Therefore, it is important to minimize the

time that a transformer operates at high temperature to maintain the long-term effective operation of meta-aramid insulation paper.
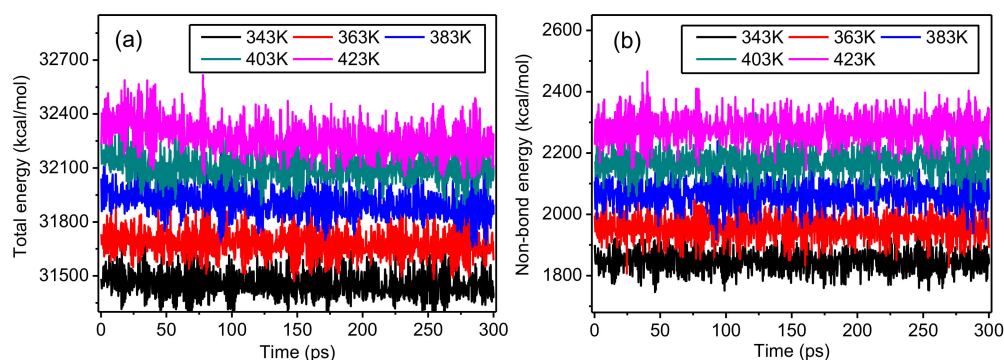

Figure 8. Changes of (**a**) total energy and (**b**) non-bond energy during the simulations at different temperatures.
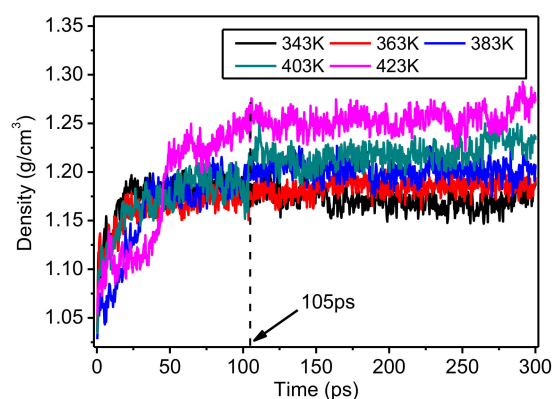

Figure 9. Change of density of amorphous regions of meta-aramid fibers during simulations at different temperatures.

Analyzing the energy changes of the crystalline and amorphous regions of meta-aramid fibers revealed that the molecular kinetic energy increased with the temperature, which caused the total energy to increase with temperature. Considering the microscale energy of a force field, the non-bond energy of crystalline regions is not greatly influenced by temperature, although a strong positive correlation exists between the non-bond energy of crystalline regions and temperature. Further analysis suggested that because the stability of the molecular structure of crystalline regions is high, atomic van der Waals forces in crystalline regions are not greatly influenced by temperature. In contrast, the molecular arrangement of amorphous regions is irregular, and the atom space is easily changed because of the strong motion of molecular chains in a thermal field. As a result, the van der Waals forces are influenced, and the non-bond energy changes. Therefore, the temperature has a stronger influence on the non-bond energy of amorphous regions than that of crystalline regions; similarly, the density change of crystalline regions with temperature is smaller than that of amorphous regions.

The thermal stability of the amorphous regions is obviously poorer than that of the crystalline regions of meta-aramid fibers, which is related to the different molecular structures in these regions. Our results indicated that the aging of meta-aramid insulation paper starts from amorphous regions with relatively poor thermal stability, and the speed of aging is influenced by the thermal field. Increasing the proportion of crystalline regions is an important approach to improve the thermal stability of meta-aramid insulation paper.

5. Analysis of Hydrogen Bonding

Hydrogen bonding is a weak force existing between or within molecules that is similar to electrostatic interactions. A hydrogen bond formed between two or more molecules is called an intermolecular hydrogen bond; a hydrogen bond formed between atoms in the same molecule is called an intramolecular hydrogen bond. The hydrogen-bonding network in a polymer influences its melting point, boiling point, structure, and cohesive energy density [43]. It is thought that the mechanical performance and aging resistance of cellulose and other materials are greatly influenced by hydrogen bonding [44]. Intramolecular hydrogen bonding plays vital roles in organisms, such as determining the helical structure of polymers and activity of biochemical molecules [45]. To prepare polymers with high molecular weight, it is necessary to mix various polymers and change the blend composition to regulate performance.

However, polymer blends are difficult to form; instead, most polymers are immiscible and form obvious interfaces with weak intercomponent bonding. Research has shown that the compatibility of immiscible copolymers can be enhanced by forming intermolecular hydrogen bonds, which can improve the performance of polymer blends [46,47]. Researchers have started to focus on the importance of hydrogen bonds since they were first recorded by an experimental method [48]. The definition of a hydrogen bond in this paper agrees with that in the literature [49].

5.1. Hydrogen Bonding in Crystalline Regions of Meta-Aramid Fibers

The hydrogen bonds formed in a crystalline area of a meta-aramid fiber are shown in Figure 10. In the crystalline area, only a hydrogen atom bonded to a nitrogen atom forms a hydrogen bond with an oxygen atom on an adjacent chain, giving a hydrogen bond with the form N–H···O, which is the same as that reported elsewhere for a meta-aramid fiber [29]. There are two forms of hydrogen bond in a crystalline area of a meta-aramid fiber [25]: one type is approximately parallel to the a-axis (Type I), and the other type is approximately parallel to the b-axis (Type II). These hydrogen bonds induce the formation of a structure similar to a three-dimensional ladder shape. This type of hydrogen bonding network has only been found in the crystalline regions of meta-aramid fibers. The existence of hydrogen bonds increases the stability of the crystalline regions. The length of Type-I hydrogen bonds is 2.25 Å, and that of Type-II hydrogen bonds is 2.10 Å in the model constructed in this paper.
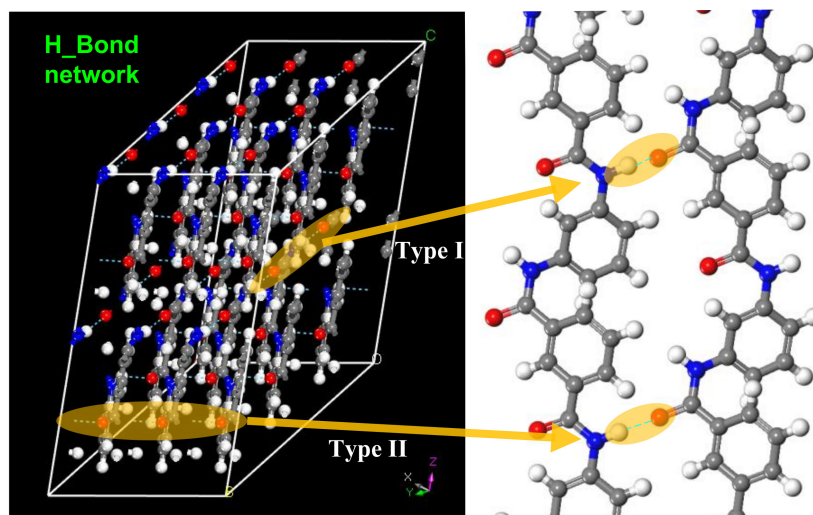

Figure 10. Hydrogen bonding network in the crystalline regions of meta-aramid fibers.

To further study the influence of temperature on the hydrogen bonding in the crystalline regions of meta-aramid fibers, statistical analysis of the hydrogen bond number and bond distance distribution was conducted; the results are presented in Figure 11a,b. Figure 11a displays the statistical results

for five repeated simulations using the initial conformation at 298 K and a fixed number of hydrogen bonds; therefore, there is no error distribution. Figure 11b shows the simulation results closest to the trend of the curve in Figure 11a.
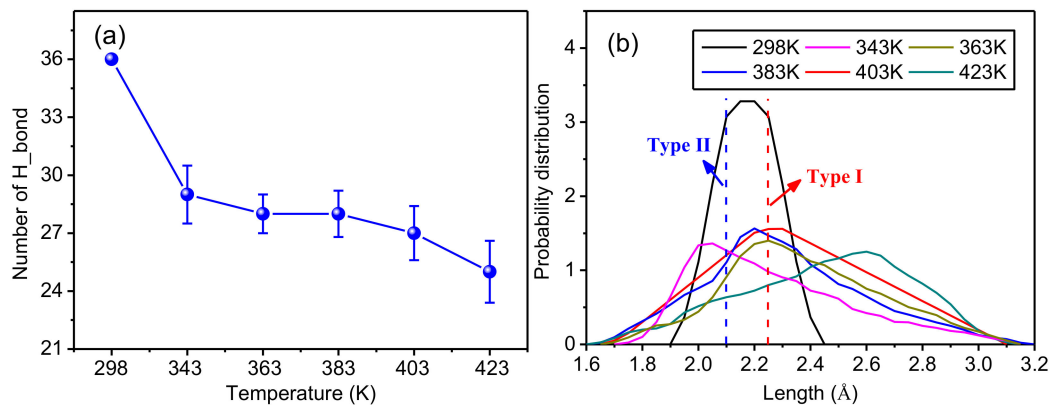

Figure 11. Influence of temperature on the hydrogen bonding network in crystalline regions of meta-aramid fibers. (**a**) Relation between temperature and the number of hydrogen bonds and (**b**) distributions of hydrogen bond lengths at different temperatures.

Figure 11a reveals that the number of hydrogen bonds in a crystalline area obviously decreases with rising temperature. This is because the structure of the crystalline area changes with rising temperature; that is, the original structure is unstable. The shift of molecular chains causes the hydrogen bond length to increase. The larger the shift of the molecular chain, the more the bond distance increased until some did not meet the conditions to form a hydrogen bond; therefore, the number of hydrogen bonds decreased with rising temperature. The original hydrogen bonding network inside the crystalline area is thus damaged because of the rising temperature. Since the existence of hydrogen bonds is an important factor maintaining the stability of the structure of crystalline regions of meta-aramid fibers, it is necessary to avoid transformer operation at high temperature for long periods.

Figure 11b shows probability distributions for the hydrogen bond lengths in the model at different temperatures; the larger the ordinate, the larger the probability that a hydrogen bond number occurs with a certain bond length. In the initial configuration, the length of Type-I and Type-II hydrogen bonds in the crystalline regions of meta-aramid fibers is distributed within the range of 1.9 Å to 2.45 Å, conforming to the distribution of actual lengths of these two types of hydrogen bond; because the bond length has only two fixed values, its distribution is the largest. After the dynamics simulations, the hydrogen bond length gradually increases on both sides of the probability distributions; in addition, the number of hydrogen bonds on the right side of the Type-I hydrogen bond is obviously greater than the number of hydrogen bonds on the left side of the Type-II hydrogen bond. That is, the number of long hydrogen bonds is greater than the number of short ones, showing that the original crystal structure has changed to some extent, and the molecular chains have shifted inside the crystalline area. However, a major proportion of the hydrogen bond lengths remained near the Type-I hydrogen bond and Type-II hydrogen bond, showing that the crystal structure has reasonable stability.

Overall, although the structure of the crystalline regions of meta-aramid fibers had pretty high stability, a thermal field may exert a certain influence; in addition, long-term operation at high temperature may degrade the structure of the crystalline regions and influence the stability of the structure of the crystalline regions to unfavorably influence the performance of meta-aramid insulation paper. Therefore, avoiding the operation of transformers at high temperature for long periods is an effective measure to guarantee the performance of meta-aramid insulation paper.

5.2. Hydrogen Bonding in Amorphous Regions of Meta-Aramid Fibers

The hydrogen bonding network that formed in an amorphous area of a meta-aramid fiber is shown in Figure 12. The hydrogen bond networks formed in the amorphous and crystalline regions are different. In the crystalline area, only the H atom on an –NH radical group and O atom on an adjacent chain formed a hydrogen bond. In addition, the molecular chains in the crystalline regions are well ordered without easy dislocation, distortion, and deformation; therefore, only an intermolecular N-H...O-type hydrogen bond could form. In contrast, the arrangement of molecular chains inside the amorphous regions is irregular, and the long chains are easily deformed, bent, and even folded; therefore, both intermolecular and intramolecular hydrogen bonds can form in the amorphous regions. The number of intermolecular hydrogen bonds was greater than that of intramolecular hydrogen bonds [50]. An N–H⋯O-type hydrogen bond can form when an O atom is close to an –NH radical group, and an N–H⋯N-type hydrogen bond can form when an N atom is close enough to an –NH radical group; these two types of hydrogen bond can be intermolecular or intramolecular. In addition, in an amorphous area, many circumstances may occur: one O atom may be close to many –NH radical groups, one –NH radical group may be close to many O atoms, one –NH radical group may be close to many –NH radical groups, or one –NH radical group may be close to an O atom, as well as an –NH radical group. The hydrogen bonds formed through such complex interactions are called unconventional or bifurcated hydrogen bonds [51]. This situation was allowed to exist in this paper.
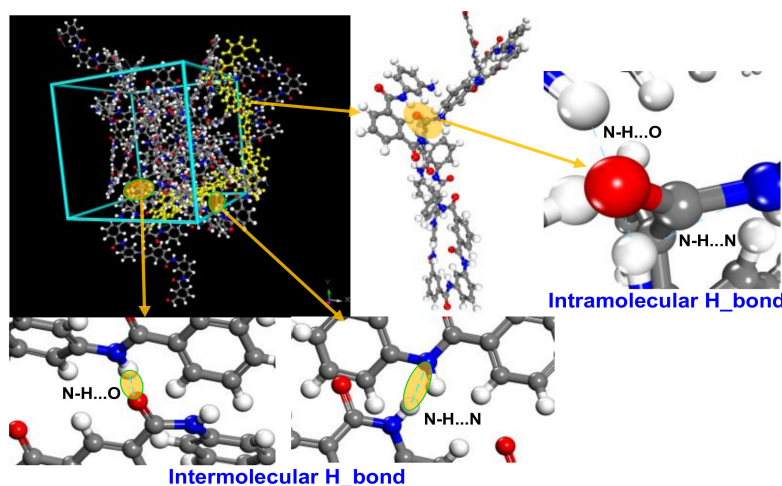

Figure 12. Hydrogen bonding network formed in an amorphous area of a meta-aramid fiber.

To further analyze the influence of temperature on hydrogen bonding in the model of the amorphous regions of meta-aramid fibers, the relation between hydrogen bond number and temperature is displayed in Figure 13a, which was obtained from repeated simulations. The hydrogen bond number of the model increases with temperature, which is mainly because the motion of fiber molecular chains is enhanced with rising temperature and the intramolecular atom space is changed, which increases the opportunity for intramolecular hydrogen bonds. With the further rise of temperature, the hydrogen bond number decreases slightly, which is mainly because the further rise of temperature further increases the chain space until the original hydrogen bonding network is damaged. In addition, the intramolecular distance can no longer meet the conditions for the formation of a hydrogen bond; therefore, the hydrogen bond number decreases slightly. The hydrogen bond number is similar for the different simulations using the model for the amorphous regions, which is consistent with reported results [50].

Figure 13b shows that the distribution of hydrogen bond lengths at room temperature (298 K) is 0.6 Å to 3.2 Å; compared with the distribution of hydrogen bond lengths at other temperatures, the distribution at room temperature is wider, and there are more short hydrogen bonds. With rising temperature, the number of long hydrogen bonds increases; all curves have pretty high peak values

when the bond length is about 2.8 Å. These results also verify that the aramid molecular chain space increases with temperature, resulting in increased atom space, less hydrogen bonds, and increased hydrogen bond length.
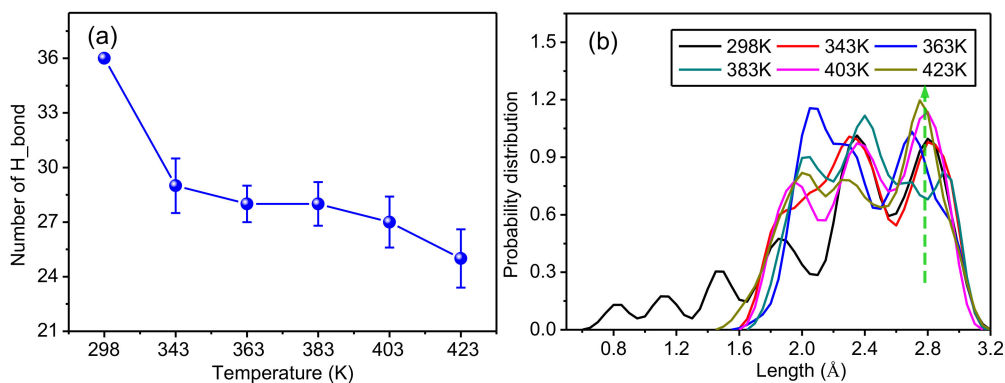

Figure 13. Influence of temperature on the hydrogen bonding network in amorphous regions of meta-aramid fibers. (**a**) Relation between temperature and hydrogen bond number and (**b**) probability distributions of hydrogen bond lengths at different temperatures.

6. Conclusions

The influence of the thermal field during the operation of a transformer on the thermal stability of meta-aramid insulation paper was studied by a molecular dynamics simulation method. The changes of chemical parameters, chain motion, hydrogen bonding, and other model parameters in crystalline and amorphous regions with temperature were analyzed, which provided the following conclusions:

1. At various temperatures, the modulus values of crystalline regions were two to three times higher than those of amorphous regions. The increased crystallinity of crystalline regions improved the modulus of meta-aramid insulation paper. Toughness may also be influenced to a certain degree. The incompressibility, rigidity, capacity to resist deformation, plasticity, and toughness of the crystalline regions were obviously higher than those of the amorphous areas, whereas the toughness of the amorphous regions was better than that of the crystalline regions. Under the action of a thermal field, the mechanical parameters in the crystalline and amorphous regions of meta-aramid fibers are different. The amorphous regions were more sensitive to temperature than the crystalline regions. The main reason for this difference is molecular structure: the molecular arrangement of crystalline regions had high regularity, whereas the molecular arrangement of amorphous regions had low regularity, and was even random.

2. The action of the thermal field slightly increased the motion of the molecular chains in the crystalline regions of meta-aramid fibers. The molecular chain motion of the amorphous regions was more sensitive to temperature than that in the crystalline regions. The aging of meta-aramid insulation paper starts from amorphous regions with relatively poor thermal stability, and its aging speed is influenced by the thermal field. An appropriate increase of the crystalline area proportion and decrease of the operating temperature of the transformer can improve the thermal stability of meta-aramid insulation paper.

3. Long-term operation at high temperature may destroy the structure of crystalline regions of meta-aramid fibers, lowering their stability and degrading the performance of meta-aramid insulation paper. The rise of temperature may change the distributions of hydrogen bond lengths in both the crystalline and amorphous regions. Type-I and Type-II hydrogen bonds were observed in the crystalline regions. The hydrogen bond length in amorphous regions increased and then gradually decreased with rising temperature.

References

1. Zhang, M.Y. Study on Relationships between Structure of Aramid Fibers and Aramid Pulp and Properties of Aramid Paper. Ph.D. Thesis, Shanxi University of Science and Technology, Xi'an, China, 2012.

2. Jain, A.; Vijayan, K. Thermally induced structural changes in nomex fibers. *Mater. Sci.* **2002**, *25*, 341–346. [CrossRef]

3. Liao, R.J.; Li, X.; Yang, L.J. Effect of the Ratios of Aramid Fiber to Pulp on the Properties of Aramid Paper. *High Volt. Eng.* **2015**, *41*, 364–373. [CrossRef]

4. Tan, Z.Q.; Qian, Y.X.; Wu, H.X.; Sun, J. Structure and properties of aramid 1313. *Synth. Fiber Ind.* **1993**, *16*, 18–21.

5. Wei, Z.; Ju F., X.; Jing, W.Z.; Chao, T.; Zhong, Y.Z. Influence of Polymethylsilsesquioxane Content to the Thermal Stability of Meta-Aramid Fiber Insulation Paper. *Materials* **2018**, *11*. [CrossRef]

6. Liu, D.; Hoang, A.T.; Pourrahimi, A.M.; Pallon, L.K.H.; Nilsson, F.; Gubanski, S.M.; Olsson, R.T.; Hedenqvist, M.S.; Gedde, U.W. Influence of nanoparticle surface coating on electrical conductivity of LDPE/Al$_2$O$_3$ nanocomposites for HVDC cable insulations. *IEEE Trans. Dielect. Electr. Insul.* **2017**, *24*, 1396–1404. [CrossRef]

7. Akhlaghi, S.; Pourrahimi, A.M.; Sjöstedt, C.; Bellander, M.; Hedenqvist, M.S.; Gedde, U.W. Effects of ageing conditions on degradation of acrylonitrile butadiene rubber filled with heat-treated ZnO star-shaped particles in rapeseed biodiesel. *Polym. Degrad. Stab.* **2017**, *138*, 27–39. [CrossRef]

8. Akhlaghi, S.; Pourrahimi, A.M.; Sjöstedt, C.; Bellander, M.; Hedenqvist, M.S.; Gedde, U.W. Degradation of fluoroelastomers in rapeseed biodiesel at different oxygen concentrations. *Polym. Degrad. Stab.* **2017**, *136*, 10–19. [CrossRef]

9. Zhang, S.; Tang, C.; Xie, J.; Zhou, Q. Improvement of thermal stability of insulation paper cellulose by modified polysiloxane grafting. *Appl. Phys. Lett.* **2016**, *109*, 1565. [CrossRef]

10. Tang, C.; Zhang, S.; Wang, Q.; Wang, X.; Hao, J. Thermal stability of modified insulation paper cellulose based on molecular dynamics simulation. *Energies* **2017**, *10*, 397. [CrossRef]

11. Li, J.; Zhang, Z.T.; Zou, P.; Yang, L.J.; Liao, R.J. Dielectric properties and thermal stability of vegetable oil-paper insulation. *J. Electr. Power Sci. Technol.* **2010**, *25*, 75–80. [CrossRef]

12. Liang, W.; Chao, T.; Shi P., Z.; Sheng, L Z. Terahertz Time Domain Spectroscopy of Transformer Insulation Paper after Thermal Aging Intervals. *Materials* **2018**, *11*, 2124. [CrossRef]

13. Yin, F.; Tang, C.; Tang, Y.; Gui, Y.; Zhao, Z. Reactive Molecular Dynamics Study of Effects of Small-Molecule Organic Acids on PMIA Thermal Decomposition. *J. Phys. Chem. B* **2018**, *122*, 10384–10392. [CrossRef] [PubMed]

14. Pathak, C.S.; Mandavgane, S.A. Application of recycle paper mill waste (rpmw) as a thermal insulation material. *Waste Biomass Valoriz.* **2018**, 1–10. [CrossRef]

15. Zhang, C.Y.; Qu, L.J.; Wang, Y.N.; Xu, T.L.; Zhang, C.L. Thermal insulation and stability of polysiloxane foams containing hydroxyl-terminated polydimethylsiloxanes. *RSC Adv.* **2018**, *8*, 9901–9909. [CrossRef]

16. Munajad, A.; Subroto, C.; Suwarno, S. Fourier transform infrared (FTIR) spectroscopy analysis of transformer paper in mineral oil-paper composite insulation under accelerated thermal aging. *Energies* **2018**, *11*, 364. [CrossRef]

17. Mazzinghi, A.; Sabbadini, M.; Freni, A. Enhanced rf behavior multi-layer thermal insulation. *Sci. Rep.* **2018**, *8*, 91. [CrossRef] [PubMed]

18. Tang, C.; Zhang, S.; Xie, J.Y.; Lv, C. Molecular simulation and experimental analysis of Al$_2$O$_3$-nanoparticle-modified insulation paper cellulose. *IEEE Trans. Dielectr. Electr. Insul.* **2017**, *24*, 1018–1026. [CrossRef]

19. Moyassari, A.; Mostafavi, H.; Gkourmpis, T.; Hedenqvist, M.S.; Gedde, U.W.; Nilsson, F. Simulation of semi-crystalline polyethylene: Effect of short-chain branching on tie chains and trapped entanglements. *Polymer* **2015**, *72*, 177–184. [CrossRef]

20. Wen, X.T.; Chao, T.; Qian, W.; Shi, L.Z.; Ya, L.Y. The Effect and Associate Mechanism of Nano SiO2 Particles on the Diffusion Behavior of Water in Insulating Oil. *Materials* **2018**, *11*, 2373. [CrossRef]

21. Anand, A.; Patey, G.N. Mechanism of urea crystal dissolution in water from molecular dynamics simulation. *J. Phys. Chem. B* **2018**, *122*, 1213–1222. [CrossRef]

22. Wang, G.M.; Sandberg, W.C. Study on Polarization/Depolarization Current Characteristic of Oil-impregnated Insulation Paper with Non-uniform Thermal Aging. *Nanotechnology* **2007**, *18*, 135702. [CrossRef] [PubMed]

23. Maxim, B.; Aleksei, A. Molecular Dynamics Simulation of DNA Capture and Transport in Heated Nanopores. *ACS Appl. Mater. Int.* **2016**, *8*, 12599–12608. [CrossRef]

24. Khajeh, A.R.A.; Shankar, K.; Choi, P. Prediction of the Active Layer Nanomorphology in Polymer Solar Cells Using Molecular Dynamics Simulation. *Appl. Mater. Int.* **2013**, *5*, 4617–4624. [CrossRef] [PubMed]

25. Cui, J.L.; Yang, L.J.; Zhou, L.; Wang, Y. Nanoscale soldering of axially positioned single-walled carbon nanotubes: A molecular dynamics simulation study. *ACS Appl. Mater. Int.* **2014**, *6*, 2044–2050. [CrossRef] [PubMed]

26. Tao, Y.H.; Xue, Q.Z.; Liu, Z.L.; Shan, M.X.; Ling, C.C.; Wu, T.T.; Li, X.F. Tunable Hydrogen Separation in Porous Graphene Membrane: First-Principle and Molecular Dynamic Simulation. *ACS Appl. Mater. Int.* **2014**, *6*, 8048. [CrossRef] [PubMed]

27. Kawaguchi, K.; Ito, H.; Kuwahara, T.; Higuchi, Y.; Ozawa, N.; Kubo, M. Atomistic Mechanisms of Chemical Mechanical Polishing of a Cu Surface in Aqueous H$_2$O$_2$: Tight-Binding Quantum Chemical Molecular Dynamics Simulations. *ACS Appl. Mater. Int.* **2016**, *8*, 11830. [CrossRef] [PubMed]

28. Xi, P.; Gao, J.; Li, W.G. *High-Tech Fiber*; Chemical Industry Press: China, Beijing, 2004.

29. Kakida, H.; Chatani, Y.; Tadokoro, H. Crystal structure of poly(m-phenylene isophthalamide). *J. Polym. Sci. Polym. Phys. Ed.* **1976**, *14*, 427–435. [CrossRef]

30. Tanaka, F.; Iwata, T. Estimation of the elastic modulus of cellulose crystal by molecular mechanics simulation. *Cellulose* **2006**, *13*, 509–517. [CrossRef]

31. Finkenstadt, V.L.; Millane, R.P. Crystal structure of valonia cellulose I-beta. *Macromolecules* **1998**, *31*, 7776–7783. [CrossRef]

32. Yang, W.; Yu, H.; Zhu, M.F.; Bai, H.W.; Chen, Y.M. Poly(m-phenylene isophthalamide) ultrafine fibers from an ionic liquid solution by dry-jet-wet-electrospinning. *J. Macromol. Sci. B* **2006**, *45*, 573–579. [CrossRef]

33. Wang, X.B.; Tang, C.; Wang, Q.; Li, X.P.; Hao, J. Selection of optimal polymerization degree and force field in the molecular dynamics simulation of insulating paper cellulose. *Energies* **2017**, *10*, 1377. [CrossRef]

34. Yu, Y.C.; Zhu, W.; Xiao, J.J.; Guo, X.; Tang, G.; Zhen, J.H.; Xiao, M. Molecular Dynamics Simulation of Binding Energies and Mechanical Properties of Energetic Systems with Four Components. *Acta Chim. Sin.* **2010**, *68*, 1181–1187. [CrossRef]

35. Yang, L.J.; Liao, R.J.; Sun, C.X.; Zhu, M.Z. Influence of vegetable oil on the thermal aging rate of kraft paper and its mechanism. *IEEE Trans. Dielectr. Electr. Insul.* **2011**, *18*, 692–700. [CrossRef]

36. Valiyaveettil, S.; Gans, C.; Klapper, M.; Gereke, R.; Müllen, K. Synthesis and structural study of poly(isophthalamide)s. *Polym. Bull.* **1995**, *34*, 13–19. [CrossRef]

37. Mazeau, K.; Heux, L. Molecular dynamics simulations of bulk native crystalline and amorphous structures of cellulose. *J. Phys. Chem. B* **2003**, *107*, 2394–2403. [CrossRef]

38. Li, X.; Tang, C.; Wang, Q.; Li, X.P.; Hao, J. Molecular simulation research on the micro effect mechanism of interfacial properties of nano SiO$_2$/meta-aramid fiber. *Int. J. Heat Technol.* **2017**, *35*, 123–129. [CrossRef]

39. Liu, D.; Pallon, L.K.H.; Pourrahimi, A.M.; Zhang, P.; Diaz, A.; Holler, M.; Schneiderd, K.; Olssona, R.T.; Hedenqvista, M.S.; Yua, S.; et al. Cavitation in strained polyethylene/aluminium oxide nanocomposites. *Eur. Polym. J.* **2017**, *87*, 255–265. [CrossRef]

40. Wu, J.L. *Elasticity*; Higher Education Press: China, Beijing, 2001.

41. Hofmann, D.; Fritz, L.; Ulbrich, J.; Paul, D. Molecular simulation of small molecule diffusion and solution in dense amorphous polysiloxanes and polyimides. *Comput. Theor. Polym. Sci.* **2000**, *10*, 419–436. [CrossRef]

42. Yang, J.S.; Yang, C.L.; Wang, M.S.; Chen, B.D.; Ma, X.G. Crystallization of alkane melts induced by carbon nanotubes and graphene nanosheets: A molecular dynamics simulation study. *Phys. Chem. Chem. Phys.* **2011**, *13*, 15476–15482. [CrossRef]

43. Zhang, S.; Tang, C.; Chen, G.; Zhou, Q.; Lv, C.; Li, X. The influence and mechanism of nano Al_2O_3 to the thermal stability of cellulose insulation paper. *Sci. Sin.* **2015**, *45*, 1167–1179. [CrossRef]

44. Heinera, A.P.; Kuuttib, L.; Telemana, O. Comparison of the interface between water and four surfaces of native crystalline cellulose by molecular dynamics simulations. *Carbohydr. Res.* **1998**, *306*, 205–220. [CrossRef]

45. Yin, K.L.; Zou, D.H.; Yang, B.; Zhang, X.H.; Xia, Q.; Xu, D.J. Investigation of H-bonding for the related force fields in materials studio software. *Comput. Appl. Chem.* **2006**, *23*, 1335–1340. [CrossRef]

46. Li, F.; Dong, J.Q.; Shen, Q. The function of hydrogen bond in polymer blends i. characters and affecting factors of hydrogen bond. *Polym. Bull.* **2009**, *35*, 54–65. [CrossRef]

47. Li, F.; Dong, J.Q.; Shen, Q. Hydrogen bonds in polymer blends II. Effects of hydrogen bonds on properties of polymer blends and methods of introduction. *Chin. Polym. Bull.* **2009**, *35*, 54–65. [CrossRef]

48. Zhang, J.; Chen, P.C.; Yuan, B.K.; Ji, W.; Cheng, Z.H.; Qiu, X.H. Real-space identification of intermolecular bonding with atomic force microscopy. *Science* **2013**, *342*, 611–614. [CrossRef] [PubMed]

49. Tang, C.; Li, X.; Li, Z.W.; Hao, J. Interfacial hydrogen bonds and their influence mechanism on increasing the thermal stability of nano-SiO_2-modified meta-aramid fibres. *Polymers* **2017**, *9*, 504. [CrossRef]

50. Yin, F.; Tang, C.; Li, X.; Hao, J. Effect of moisture on mechanical properties and thermal stability of meta-aramid fiber used in insulating paper. *Polymers* **2017**, *9*, 537. [CrossRef]

51. Zhang, G.H.; Ma, W.X.; Wan, H.J. The type and nature of hydrogen bonds. *Chem. Teach.* **2007**, *7*, 72–75.